




Temperature-dependent phase lag and non-local thermoelastic damping and frequency shift in thermoelastic plates

R. Kumar , P. Singhal 

Kurukshetra University, Kurukshetra, India

 poojaacad009@gmail.com

ABSTRACT

Thermoelastic damping and frequency shift are critical factors influencing the performance and stability of micro- and nano-scale resonators, such as those employed in MEMS and NEMS devices. Traditional thermoelastic models often overlook important scale-dependent behaviors, thermal relaxation effects, and material property variations with temperature, leading to inaccuracies at small scales. To address these limitations, the present study investigates thermoelastic damping and frequency shift in a Kirchhoff plate resonator by incorporating non-local elasticity theory, the dual-phase lag heat conduction model, and temperature-dependent material properties. In order to investigate thermoelastic damping and frequency shift of Kirchhoff plate resonator, the current work takes into account the influence of non-local, dual phase lag, and temperature dependent properties on thermoelastic theory. The governing equations, comprise equations of motion and heat conduction equation which include a temperature-dependent property, a dual-phase lag model along with non-local parameters are formulated with the assistance of Kirchhoff-Love plate theory. Under the simply supported boundary conditions, thermoelastic damping and frequency shift are analysed. The derived amounts are graphically displayed with different thickness and length values. The current work additionally deduces a specific example of interest. Results are graphically presented to illustrate key trends, and a specific numerical example is discussed to demonstrate the applicability of the model. This study enhances the accuracy of thermoelastic analysis in micro-scale resonator design by integrating advanced theoretical considerations often neglected in conventional models.

KEYWORDS

thermoelastic • Kirchhoff-Love plate theory • non-local dual-phase-lag model • TDP model • frequency shift thermoelastic damping

Citation: Kumar R, Singhal P. Temperature-dependent phase lag and non-local thermoelastic damping and frequency shift in thermoelastic plates. *Materials Physics and Mechanics*. 2025;53(3): 94–115.

http://dx.doi.org/10.18149/MPM.5332025_8

Introduction

It is well known that in many cases, non-uniform beams may achieve a better distribution of strength and weight than uniform beams and sometimes, it satisfies special architectural and functional requirements. Therefore, the static and dynamic analysis of beams with variable thickness has been the subject of numerous investigations because of its relevance to aeronautical, civil, and mechanical engineering. Most studies are available on variable thickness beams based on either the Euler beam or the Timoshenko beam theory.

In many advanced materials and microscale systems, the interaction between an external electric field and charge carriers is governed by the mutual competition between two dynamic processes: the electromagnetic field propagation and the carrier transport



dynamics (e.g., drift, diffusion, or thermal motion). The electric field tends to polarize the medium and accelerate charge carriers, while the carriers themselves, influenced by temperature gradients and scattering mechanisms, redistribute and modulate the local field. This interplay creates a feedback loop that can significantly influence heat conduction, damping behavior, and the dynamic response of thermoelastic systems. At micro- and nano-scales, where quantum and non-local effects become significant, the delayed response of heat carriers and non-uniform charge distribution due to size confinement can lead to non-intuitive behavior, such as enhanced damping or frequency shifts.

Thermoelastic damping (TD) is a form of structural damping that arises from the interaction between thermal and mechanical fields. In a bending thermoelastic structure, the inner side of the bend experiences compression while the outer side experiences tension. This interaction between the thermal and mechanical fields creates a thermal gradient, which results in irreversible heat generation within the structure. This heat generation subsequently leads to entropy production and ultimately causes energy dissipation.

The mechanism and magnitude of linear thermoelastic damping (TD) in a flexural vibrating thin beam have been extensively investigated. TD is commonly assessed using the inverse of the quality factor (Q) [1,2] established the theoretical basis for TD and formulated an expression to calculate the quality factor for a thin beam oscillating in its flexural mode. Thermoelastic damping in micro-beam resonators was discussed by [3].

Conventional continuum theories are often unsuitable for accurately describing the behavior of nanostructures with extremely small characteristic sizes but nonlocal continuum theories effectively describe material properties from microscopic scales up to the size of the lattice parameter, thus providing a satisfactory explanation for certain atomic-scale phenomena. In [4], it was developed non local theory of elasticity. In [5], it was introduced theory of nonlocal thermoelasticity in which stress at a point x in a continuous body is not solely determined by the strain at that point, but also by the strains at all surrounding points. In study [6], it was expected to be helpful for the theoretical modeling of thermoelasticity at the nano-scale and may be beneficial for the design of nano-sized and multi-layered devices.

Currently, most investigations into thermoelastic damping (TD) assume that material properties are temperature-independent. However, for many materials, properties such as the modulus of elasticity, thermal conductivity, and specific heat actually vary with temperature. To thoroughly examine the interaction between thermal and mechanical fields, it is essential to consider the impact of temperature-dependent material properties, even within a narrow temperature range.

The elasticity solution for the clamped- simply supported beams with variable thickness was presented in [7]. In [8], it was investigated the thermoelastic damping of vibrations in arbitrary direction in coupled thermoelastic plate. In [9], it was studied the transverse vibration in piezothermoelastic beam resonator, based on Euler-Bernoulli theory for clamped and free end conditions. In [10], it was developed a size- dependent Bernoulli-Euler beam formulation on the basis of new model of couple stress theory and prepared the mathematical formulation for clamped (C-C), simply supported (S-S) and cantilever (C-F) boundary conditions.

The influence of heat sources and relaxation time on temperature distribution in tissues was studied in [11]. In [12], it was studied the exact solution of thermoelastic

damping and frequency shifts in a nano-beam resonator. In [13], it was explored the damping characteristics in microscale modified couple stress thermoelastic circular Kirchhoff plate resonators. In [14], it was introduced effect of temperature dependent material properties on thermoelastic damping in thin beams. Some results in Moore-Gibson-Thompson thermoelasticity of dipolar bodies are examined in [15]. In [16], it was studied the thermoelastic damping in nonlocal nanobeams considering dual-phase-lagging effect. The response of nanobeams with TDP Using State-Space Method via modified couple stress theory was described in [17]. In [18], it was discussed the thermoelastic damping and frequency shift in Kirchhoff plate resonators based on modified couple stress theory with dual-phase-lag model. Study [19] focused frequency shifts and thermoelastic damping in different types of nano-/Micro-scale beams with sandiness and voids under three thermoelasticity theories. A combined model for power generation planning with reserve dispatch and weather uncertainties including penetration of renewable sources was presented in [20]. In [21], it was proposed a model for a micro-grid architecture incorporating the role of aggregators and renewable sources on the prosumer side, working together to optimize configurations and operations. The frequency shifts and thermoelastic damping in distinct micro/nano-scale piezothermoelastic fiber-reinforced composite beams under examined some three heat conduction models were presented in [22]. In [23], it was explored functionally graded nonlocal thermoelastic nanobeam with memory-dependent derivatives. In [24], it were discussed the effects of two temperature and laser pulse on modified couple stress thermoelastic diffusion beam. In [25], it were provided analytical modeling and numerical analysis of thermoelastic damping in ultrathin elastic films due to surface effects. In [26], it was analysed the magneto-thermoelastic vibrations of rotating Euler–Bernoulli nanobeams using the nonlocal elasticity model. A buckling analysis of thermoelastic micro/nano-beams considering the size-dependent effect and non-uniform temperature distribution was provided in [27]. In [28], it was discussed the vibration of piezo-magneto-thermoelastic nanobeam submerged in fluid with variable nonlocal parameter. In [29], it was computed phase velocities, attenuation coefficients, specific loss, penetration depth and construct the fundamental solution of the system of differential equations in the theory of an electro-microstretch viscoelastic solids in case of steady oscillations in terms of elementary functions. The propagation of Lamb waves in a homogeneous isotropic thermoelastic micropolar solid with two temperatures bordered with layers or half-spaces of inviscid liquid subjected to stress free boundary conditions was studied in [30]. In [31], it was constructed fundamental solution for the system of differential equations for steady oscillations in terms of elementary functions. A novel technique is used to study the magnetic field influence in the free surface of an elastic semiconductor medium for a one- dimensional (1D) deformation during the hyperbolic two-temperature theory to study the coupled between the plasma, thermo-elastic waves was proposed in [32]. Study [33] examined the interaction between the magnetic field and the excited semiconductor medium during the microtemperature process. In [34], it was studied the effect of Hall current of elastic semiconductor medium, when the medium is exposed to very strong magnetic field. In [35], it was presented the graphical comparison by showing that the exact and numerical solutions nearly coincide with each other. The electro-magnetic-thermal-microstretch elastic mathematical-physical model of semiconductor medium was investigated in [36]. In [37], it was formulated a novel

model of a microelongated semiconductor material. Thermal and elastic interactions in isotropic microplate resonators with elastic and viscous properties, exhibiting Kelvin–Voigt behavior, under a uniform magnetic field were investigated in [38]. In [39], it was examined the modeling of the transient thermodynamic reaction of a Kirchhoff–Love thermoelastic thin circular plate that is simply supported and set on an elastic base of Winkler type. In [40], it was found that the initial stress and the fractional parameter significantly influences the varieties of field amounts. A model that is highly effective in properly depicting the unusual thermal conductivity phenomena often found in nanoscale devices was proposed in [41]. In [42], it was examined the thermoelastic behavior of functionally graded (FG) materials using a partially modified thermoelastic heat transfer model.

Basic equations

Following [6,43] the governing equation in generalized thermoelastic dual-phase-lag model without body forces and heat sources are:

Constitutive relations:

$$t_{ij} = \lambda e_{kk} \delta_{ij} + 2\mu e_{ij} - \beta T \delta_{ij}. \quad (1)$$

Equations of motion:

$$(\lambda + \mu) \nabla(\nabla \cdot \vec{u}) + \mu \nabla^2 \vec{u} - \beta \nabla T = \rho(1 - \xi_1^2 \nabla^2) \frac{\partial^2 \vec{u}}{\partial t^2}. \quad (2)$$

Equation of heat conduction:

$$K \left(1 + \tau_T \frac{\partial}{\partial t}\right) \nabla^2 T = \left(1 - \xi_2^2 \nabla^2 + \tau_q \frac{\partial}{\partial t} + \frac{\tau_q^2}{2} \frac{\partial^2}{\partial t^2}\right) \left(\rho C_e \frac{\partial T}{\partial t} + \beta T_0 \frac{\partial e_{kk}}{\partial t}\right), \quad (3)$$

where

$$e_{ij} = \frac{1}{2}(u_{i,j} + u_{j,i}). \quad (4)$$

Additionally, in Eqs. (1)–(4), the constants Lamé are λ and μ . Kronecker's delta is δ_{ij} , the components of stress tensor is t_{ij} , and the components of strain tensor is e_{ij} , $\beta = (3\lambda + 2\mu) \alpha_t$, the coefficients of linear thermal expansion are α_t respectively, the temperature change is denoted by T , the displacement vector is u , the density is ρ , the Laplacian operator is Δ , and the del operator is ∇ . The coefficient of the thermal conductivity is K , the non-local parameters are represented by ξ_1, ξ_2 , the specific heat at constant strain is represented by C_e , and the reference temperature is T_0 , is assumed to be such that $T/T_0 \ll 1$. The phase lags of the temperature gradient and the heat flux are denoted by τ_T and τ_q respectively.

To explore the impact of temperature dependent property, the following assumptions are taken as: $\lambda = \lambda_0 f(t)$; $\mu = \mu_0 f(t)$, $k = k_0 f(t)$; $\beta = \beta_0 f(t)$, $E = E_0 f(t)$, where $f(t) = 1(1 - \alpha^* T_0)$, α^* is the empirical material constant and $f(t) = 1$ for the temperature independent material.

Formulation of the problem

Let us examine a non-local thermoelastic Kirchhoff plate with temperature dependent properties and dual phase lag resonators that have uniform thickness h . The center of the plate is where the Cartesian coordinate system (x , y , and z) originates. When the plate is in equilibrium, it is not under any stress or strain and maintains a constant temperature of T_0 throughout. The temperature $T(x, y, z, t)$, the displacement components $u(x, y, z, t)$,

$v(x, y, z, t)$, and $w(x, y, z, t)$ are defined. The displacement components, as per Kirchhoff's-Love Plate theory, are provided by:

$$u = -z \frac{\partial w}{\partial x}, \quad v = -z \frac{\partial w}{\partial y}, \quad w(x, y, z, t) = w(x, y, t). \quad (5)$$

Following [44], the strain and stress components are taken as:

$$\varepsilon_{xx} = -z \frac{\partial^2 w}{\partial x^2}, \quad (6)$$

$$\varepsilon_{yy} = -z \frac{\partial^2 w}{\partial y^2}, \quad (7)$$

$$\gamma_{xy} = -2\mu_0 f(t) z \frac{\partial^2 w}{\partial x \partial y} = -\frac{E_0 f(t) z}{(1+\nu)} \frac{\partial^2 w}{\partial x \partial y}, \quad (8)$$

$$t_{xx} = \frac{E_0 f(t)}{(1-\nu^2)} (\varepsilon_{xx} + \nu \varepsilon_{yy} - (1+\nu) \alpha_T T), \quad (9)$$

$$t_{yy} = \frac{E_0 f(t)}{(1-\nu^2)} (\varepsilon_{yy} + \nu \varepsilon_{xx} - (1+\nu) \alpha_T T), \quad (10)$$

where E_0 and ν_0 is Young's modulus and the Poisson ratio respectively, which are given by:

$$E_0 = \mu_0 (3\lambda_0 + 2\mu_0) / (\lambda_0 + \mu_0), \quad (11)$$

$$\nu_0 = \lambda_0 / 2(\lambda_0 + \mu_0). \quad (12)$$

Following [44,45], the bending and torsion moments are defined as follows:

$$M_x = \int_{-h/2}^{h/2} t_{xx} z dz, \quad (13)$$

$$M_y = \int_{-h/2}^{h/2} t_{yy} z dz, \quad (14)$$

$$M_{xy} = \int_{-h/2}^{h/2} t_{xy} z dz = M_{yx}. \quad (15)$$

Equations (13)–(15) recast with the aid of Eqs. (5)–(10), as:

$$M_x = -D^* \left(\frac{\partial^2 w}{\partial x^2} + \nu_0 \frac{\partial^2 w}{\partial y^2} + \alpha_T M_T (1+\nu) \right), \quad (16)$$

$$M_y = -D^* \left(\frac{\partial^2 w}{\partial y^2} + \nu_0 \frac{\partial^2 w}{\partial x^2} + \alpha_T M_T (1+\nu) \right), \quad (17)$$

$$M_{xy} = -\frac{\partial^2 w}{\partial x \partial y} (D^* (1-\nu_0)), \quad (18)$$

where $D^* = E_0 f(t) h^3 / 12 (1-\nu_0^2)$ is the flexural rigidity of the plate.

The equations for shear force resultants are:

$$Q_x = \frac{\partial M_x}{\partial x} + \frac{\partial M_{xy}}{\partial y}, \quad Q_y = \frac{\partial M_y}{\partial y} + \frac{\partial M_{xy}}{\partial x}. \quad (19)$$

The equation of motion (force equilibrium z in the direction) is given as:

$$\frac{\partial Q_x}{\partial x} + \frac{\partial Q_y}{\partial y} - \rho h (1 - \xi_1^2 \nabla^2) \frac{\partial^2 w}{\partial t^2} = 0. \quad (20)$$

Using Eqs. (16)–(18) in Eqs. (19), (20), then the equation of motion for micro plate with symmetry about y -axes is taken as:

$$D^* \frac{\partial^4 w}{\partial x^4} + \frac{E_0 f(t) \alpha_T}{(1-\nu_0) \beta d} \frac{\partial^2 M_T}{\partial x^2} + \rho h (1 - \xi_1^2 \nabla^2) \frac{\partial^2 w}{\partial t^2} = 0. \quad (21)$$

The thermal moment is given by:

$$M_T = \beta_0 f(t) d \int_{-h/2}^{h/2} T z dz. \quad (22)$$

The heat conduction equation is:

$$k_0 f(t) \left(1 + \tau_T \frac{\partial}{\partial t} \right) \nabla^2 T = \left(1 - \xi_2^2 \nabla^2 + \tau_q \frac{\partial}{\partial t} + \frac{\tau_q^2}{2} \frac{\partial^2}{\partial t^2} \right) \left(\rho c_e \frac{\partial T}{\partial t} - T_0 \beta_0 f(t) z \frac{\partial^3 w}{\partial x^2 \partial t} \right), \quad (23)$$

where

$$\nabla^2 = \frac{\partial^2}{\partial x^2} + \frac{\partial^2}{\partial z^2}. \quad (24)$$

For further simplification, the following non-dimensional quantities are taken as:

$$(x', z', u', w') = (x, z, u, w)/L, (\tau'_q, \tau'_T, t') = (\tau_q, \tau_T, t)v/L, T' = T/T_0,$$

$$M'_T = M_T/d\beta T_0 h^2, v_0'^2 = E/\rho, \xi'_1 = \xi_1/L, \xi'_2 = \xi_2/L, Q'_1 = \mu_0 Q'.$$

Equations (21) and (23) taking into account Eq. (24) reduce to the form:

$$\frac{\partial^4 w}{\partial x^4} + a_1 \frac{\partial^2 M_T}{\partial x^2} + a_2 (1 - \xi_1^2 \nabla^2) \frac{\partial^2 w}{\partial t^2} = 0, \quad (25)$$

$$a_3 \left(1 + \tau_T \frac{\partial}{\partial t}\right) \left(\frac{\partial^2 T}{\partial x^2} + \frac{\partial^2 T}{\partial z^2}\right) - \left(1 - \xi_2^2 \nabla^2 + \tau_q \frac{\partial}{\partial t} + \frac{\tau_q^2}{2} \frac{\partial^2}{\partial t^2}\right) \left(a_4 \frac{\partial T}{\partial t} - z \frac{\partial^3 w}{\partial x^2 \partial t}\right) = 0, \quad (26)$$

$$\text{where } a_1 = \frac{E\alpha_T T_0 h^2 L}{(1-\nu)D^*}, a_2 = \frac{\rho h v^2 L^2}{D^*}, a_3 = \frac{k_0}{Lv\beta_0}.$$

Following [46], the solution of Eqs. (25) and (26) for time harmonic vibrations are taken as:

$$w(x, t) = W(x)e^{i\omega t}, T(x, z, t) = \Theta(x, z)e^{i\omega t}. \quad (27)$$

where ω denotes the frequency of the plate.

Substituting the values of T from Eq. (27) in Eq. (22):

$$M_T = \beta d \int_{-h/2}^{h/2} \Theta(x, z) z dz. \quad (28)$$

Making use of Eq. (28) in Eqs. (25) and (26) yield:

$$\frac{\partial^4 W}{\partial x^4} + a_1 \frac{\partial^2 M_\theta}{\partial x^2} - \omega^2 a_2 (1 - \xi_1^2 \nabla^2) W = 0, \quad (29)$$

$$a_3 (1 + \tau_T i\omega) \left(\frac{\partial^2 \Theta}{\partial x^2} + \frac{\partial^2 \Theta}{\partial z^2}\right) = i\omega \left(1 - \xi_2^2 \nabla^2 + \tau_q i\omega - \frac{\omega^2}{2} \tau_q^2\right) \left(a_4 \Theta - z \frac{\partial^2 W}{\partial x^2}\right). \quad (30)$$

Thermal field on the thickness direction

The thermal gradient of the plate is very small as compared to that along its thickness direction:

$$\left|\frac{\partial \Theta}{\partial x}\right| \ll \left|\frac{\partial \Theta}{\partial z}\right|, \frac{\partial^2}{\partial z^2} \left[z \frac{\partial^2 W}{\partial x^2}\right] \approx 0. \quad (31)$$

With these considerations Eq. (30) take the form:

$$\frac{\partial^2 \Theta}{\partial z^2} + R_1^2 \Theta + R_2 z \frac{\partial^2 W}{\partial x^2} = 0, \quad (32)$$

where

$$R_1^2 = \frac{-a_4 \tau_q^* i\omega}{a_3 + i\omega \tau_t^*}, R_2 = \frac{i\omega \tau_q^*}{a_4 + i\omega \tau_t^*}, \tau_t^* = a_3 \tau_T + \xi_2^2 a_4, \tau_q^* = \left(1 + \tau_q i\omega - \frac{\omega^2}{2} \tau_q^2\right). \quad (33)$$

In this case, it is assumed that there is no heat across the upper and lower surfaces of the plate, then:

$$\frac{\partial \Theta}{\partial z} = 0, \quad z = \pm \frac{h}{2}. \quad (34)$$

Using conditions of Eq. (34), the general solution of Eq. (30) is written as:

$$\Theta(x, z) = -\frac{R_2}{R_1^2} \left(z - \frac{\sin(R_1 z)}{R_1 \cos(R_1 h/2)}\right) \frac{\partial^2 W}{\partial x^2}. \quad (35)$$

Inserting the value of Θ from Eq. (35) in Eq. (28) yield:

$$M_T = \beta d \int_{-h/2}^{h/2} -\frac{R_2}{R_1^2} \left(z - \frac{\sin(R_1 z)}{R_1 \cos(R_1 h/2)}\right) \frac{\partial^2 W}{\partial x^2} z dz. \quad (36)$$

The above equation takes the form:

$$M_T = \frac{-\beta d R_2 h^3}{12 R_1^2} [1 + f(R_1)] \frac{\partial^2 W}{\partial x^2}, \quad (37)$$

where $f(R_1)$ is a complex function expressed as below:

$$f(R_1) = \frac{24}{R_1^3 h^3} \left(\frac{R_1 h}{2} - \tan \frac{R_1 h}{2}\right). \quad (38)$$

From Eq. (37):

$$\frac{\partial^2 M_\theta}{\partial x^2} = -\frac{\beta d R_2 h^3}{12 R_1^2} (1 + f(R_1)) \frac{\partial^4 W}{\partial x^4}. \quad (39)$$

Equation (39) with the aid of Eq. (28) yield:

$$\frac{d^4 W}{dx^4} - a_1 \frac{\beta d R_2 h^3}{12 R_1^2} (1 + f(R_1)) \frac{\partial^4 W}{\partial x^4} - \omega^2 a_2 \left(1 - \xi_1^2 \left(\frac{\partial^2}{\partial x^2} + \frac{\partial^2}{\partial z^2} \right) \right) W = 0. \quad (40)$$

Simplifying Eq. (40) with the aid of Eq. (31):

$$D_\omega^* \frac{d^4 W}{dx^4} + \omega^2 a_2 \xi_1^2 \frac{d^2 W}{dx^2} - \omega^2 a_2 W = 0, \quad (41)$$

where

$$D_\omega^* = (1 + \varepsilon(1 + f(R_1))); \varepsilon = -\frac{a_1 \beta d R_2 h^3}{12 R_1^2}. \quad (42)$$

For the isothermal state of Nano beam Eq. (41) takes the following form:

$$\frac{d^4 W}{dx^4} + \omega_0^2 a_2 \xi_1^2 \frac{d^2 W}{dx^2} - \omega_0^2 a_2 W = 0, \quad (43)$$

where ω_0 refers to the nonlocal isothermal frequency.

Solution of Eq. (43) yields:

$$(x) = C_1 \sin \lambda_1 x + C_2 \cos \lambda_1 x + C_3 \sinh \lambda_2 x + C_4 \cosh \lambda_2 x, \quad (44)$$

where C_1, C_2, C_3, C_4 are constants.

Substitution Eq. (44) in Eq. (43) yields:

$$\omega_0^2 = \frac{\lambda_1^4}{(1 + \lambda_1^2 \xi_1^2) a_2} = \frac{\lambda_2^4}{(1 - \lambda_2^2 \xi_1^2) a_2}. \quad (45)$$

Boundary conditions

It is taken into consideration that a micro plate whose ends are either clamped-clamped (CC), simply supported (SS), clamped-clamped (CC) and clamped free (CF) in which case the following boundary conditions for the two sets [44]:

$$\text{Case (i) For Clamped-Clamped (CC): } W = 0, \frac{\partial W}{\partial x} = 0, x = 0, L. \quad (46)$$

$$\text{Case (ii) For Simply Supported (SS): } W = 0, \frac{\partial^2 W}{\partial x^2} = 0, x = 0, L. \quad (47)$$

$$\text{Case (iii) For Clamped Supported (CS): } W = 0, \frac{\partial W}{\partial x} = 0, \frac{\partial^2 W}{\partial x^2} = 0, x = 0, L. \quad (48)$$

$$\text{Case (iv) For Clamped Free (CF): } W = 0, \frac{\partial W}{\partial x} = 0, \text{ at } x = 0, \frac{\partial^2 W}{\partial x^2} = 0, \frac{\partial^3 W}{\partial x^3} = 0, x = L. \quad (49)$$

Substituting Eq. (44) in the boundary conditions Eqs. (46)–(49), the following set of frequency equations are obtained:

$$\text{CC: Case (i). } 2 \cos \lambda_1 L \cosh \lambda_2 L + \left(\frac{\lambda_1}{\lambda_2} - \frac{\lambda_2}{\lambda_1} \right) \sin \lambda_1 L \sinh \lambda_2 L - 2 = 0. \quad (50)$$

$$\text{SS: Case (ii). } \sin(\lambda_1 L) = 0. \quad (51)$$

$$\text{CS: Case (iii). } \lambda_2 \sin \lambda_1 L \cosh \lambda_2 L - \lambda_1 \sinh \lambda_2 L \cos \lambda_1 L = 0. \quad (52)$$

$$\text{CF: Case (iv). } 2 \cos \lambda_1 L \cosh \lambda_2 L + \left(\frac{\lambda_1}{\lambda_2} - \frac{\lambda_2}{\lambda_1} \right) \sin \lambda_1 L \sinh \lambda_2 L + \left(\frac{\lambda_1^2}{\lambda_2^2} + \frac{\lambda_2^2}{\lambda_1^2} \right) = 0. \quad (53)$$

Take note that Eq. (45) describes the relationship between λ_1 and λ_2 . These transcendental equations can be solved, and the nonlocal isothermal frequency ω_0 of each boundary condition can be found by substituting the solutions into Eq. (45).

Making use of Eq. (44) in boundary condition Eq. (47) yield:

$$\sin(\lambda_1 L) = 0. \quad (54)$$

From above equation $\lambda_1 = \frac{n\pi}{L}, n \in I$.

Comparing Eq. (41) and Eq. (43) gives the following relation between ω and ω_0 :

$$\omega = \omega_0 \sqrt{1 + \varepsilon(1 + (f(R_1)))}. \quad (55)$$

Given that the relaxation strength value is often small ($\varepsilon \ll 1$), the right-hand side of Eq. (55) can be expanded to the first order as shown below:

$$\omega = \omega_0 \left[\left(1 + \frac{\varepsilon}{2} (1 + f(\omega_0)) \right) \right], \quad (56)$$

$$f(\omega_0) = \frac{24}{R_1^3 h^3} \left(\frac{R_1 h}{2} - \tan \frac{R_1 h}{2} \right). \quad (57)$$

From Eq. (32), since the quantity R_1^2 in Eq. (33) is complex in nature, the following equations can be obtained by applying Euler's theorem:

$$R_1 = R_0 e^{\frac{-i\theta}{2}}, R_0 = \sqrt{\frac{s_0^*}{L_2^*}}, \theta = \tan^{-1} \left[-\frac{\omega^3 \rho c_e \tau_q L v R^* - K L_1^*}{K \omega^2 \rho c_e \tau_q L v + \omega R^* L_1^*} \right], \quad (58)$$

where $s_0^* = \sqrt{(K^2 + \omega^2 R^{*2})(\omega^4 \rho^2 c_e^2 \tau_q^2 L^2 v^2 + L_1^{*2})}$, $R^* = K \tau_T + \xi_2^2 \rho c_e L v$,

$$L_1^* = \left(\frac{\omega^3}{2} \rho c_e L v \tau_q^2 - \omega \rho c_e \right), L_2^* = K^2 + \omega^2 R^{*2}.$$

Replace ω with ω_0 in Eq. (58):

$$R_1 = \sqrt{2} p_1 \left(\cos \frac{\theta}{2} - i \sin \frac{\theta}{2} \right), \quad (59)$$

and

$$p_1 = \sqrt{\frac{\sqrt{(K^2 + \omega_0^2 R^{*2})(\omega_0^4 \rho^2 c_e^2 \tau_q^2 L^2 v^2 + L_1^{*2})}}{2(K^2 + \omega_0^2 R^{*2})}}, \theta = \tan^{-1} \left[-\frac{\omega_0^3 \rho c_e \tau_q L v R^* - K L_1^*}{K \omega_0^2 \rho c_e \tau_q L v + \omega_0 R^* L_1^*} \right]. \quad (60)$$

The frequency ω is complex in nature and hence:

$$\omega_n = \omega_R^m + i \omega_I^m, \omega_R^m = \text{Re}(\omega_n), \omega_I^m = \text{Im}(\omega_n), \quad (61)$$

$$\omega_R^n = \omega_0 \left[1 + \frac{\varepsilon}{2} \left\{ \left(1 + \frac{6 \cos \theta}{(p_1 h)^2} - \frac{6 \sqrt{2} \cos \frac{3\theta}{2}}{(p_1 h)^3} \left(\frac{\sin \zeta_1 + \tan \frac{3\theta}{2} \sinh(\zeta_1 \zeta_2)}{\cos \zeta_1 + \cosh(\zeta_1 \zeta_2)} \right) \right\} \right], \quad (62)$$

$$\omega_I^n = \frac{\varepsilon}{2} \left\{ \frac{6 \sin \theta}{(p_1 h)^2} - \frac{6 \sqrt{2} \cos \frac{3\theta}{2}}{(p_1 h)^3} \left(\frac{\sin \zeta_1 \tan \frac{3\theta}{2} - \sinh(\zeta_1 \zeta_2)}{\cos \zeta_1 + \cosh(\zeta_1 \zeta_2)} \right) \right\}, \quad (63)$$

where, $\zeta_1 = \sqrt{2} p_1 h \cos \frac{\theta}{2}$, $\zeta_2 = \tan \frac{\theta}{2}$.

The thermoelastic damping and frequency shift in a thermoelastic circular plate are understood as follows [47]:

$$Q^{-1} = 2 \left| \frac{\text{Im}(\omega_n)}{\text{Re}(\omega_n)} \right|, \quad (64)$$

$$\omega_s = \left| \frac{\text{Re}(\omega_n) - \omega_0}{\omega_0} \right|. \quad (65)$$

Numerical results and Discussion

Equations (64) and (65) were utilized to calculate the thermoelastic damping Q^{-1} and frequency shift ω_s of the initial two vibration modes, both in the absence and presence of pair stress. MATLAB software has been utilized to perform numerical computations on magnesium material. For simply supported plates with different thickness and length values, the computed simulated results are shown graphically in Figs. 1–16 and in Tables 1–10 below.

Following [24]: $\rho = 1.74 \cdot 10^3$, $C_e = 1.0400$, $\lambda = 2.696 \cdot 10^{10}$, $\mu = 1.639 \cdot 10^{10}$, $K = 1.70 \cdot 10^2$, $T = 293$, $\alpha_t = 1.78 \cdot 10^{-5}$, $\tau_t = 0.04$, $\tau_q = 0.02$, $\omega = 10$.

The damping values are presented in Table 1 for different lengths and with varying values of the non-local parameter ξ_1 . The table includes lengths up to 45.2, with ξ_1 varying from 0 to 0.8, while ξ_2 is fixed at 0.04. An increase in the damping value is observed within the range of $2.32 \cdot 10^{-5}$ to $1.90 \cdot 10^{-2}$ as the length changes from 5.2 to 25.2 for $\xi_1 = 0.4$. Similarly, damping increases with the increase in ξ_1 for the same length. For instance, the damping value is $1.82 \cdot 10^{-4}$ for a length of 20.2 and $\xi_1 = 0$; this increases to $1.95 \cdot 10^{-2}$ for $\xi_1 = 0.8$ for the same length.

Table 1. Damping for different lengths keeping fixed $\xi_2 = 0.04$

$\xi_1 \backslash L$	0.2	5.2	10.2	15.2	20.2	25.2	30.2	35.2	40.2	45.2
0	$4.32 \cdot 10^{-22}$	$6.52 \cdot 10^{-6}$	$1.32 \cdot 10^{-7}$	$1.40 \cdot 10^{-5}$	$1.82 \cdot 10^{-4}$	$1.85 \cdot 10^{-3}$	$2.93 \cdot 10^{-3}$	$4.56 \cdot 10^{-3}$	$8.87 \cdot 10^{-3}$	$3.45 \cdot 10^{-2}$
0.4	$7.66 \cdot 10^{-21}$	$2.32 \cdot 10^{-5}$	$8.52 \cdot 10^{-4}$	$3.11 \cdot 10^{-3}$	$8.61 \cdot 10^{-3}$	$1.90 \cdot 10^{-2}$	$3.53 \cdot 10^{-2}$	$5.99 \cdot 10^{-2}$	$9.15 \cdot 10^{-2}$	$1.28 \cdot 10^{-1}$
0.6	$5.82 \cdot 10^{-20}$	$8.26 \cdot 10^{-5}$	$1.78 \cdot 10^{-3}$	$5.95 \cdot 10^{-3}$	$1.45 \cdot 10^{-2}$	$3.08 \cdot 10^{-2}$	$5.76 \cdot 10^{-2}$	$9.33 \cdot 10^{-2}$	$1.37 \cdot 10^{-1}$	$1.91 \cdot 10^{-1}$
0.8	$2.45 \cdot 10^{-19}$	$1.83 \cdot 10^{-4}$	$2.59 \cdot 10^{-3}$	$8.24 \cdot 10^{-3}$	$1.95 \cdot 10^{-2}$	$4.44 \cdot 10^{-2}$	$8.27 \cdot 10^{-2}$	$1.36 \cdot 10^{-1}$	$2.08 \cdot 10^{-1}$	$3.04 \cdot 10^{-1}$

Table 2 illustrates the variation of frequency shift for different lengths with various values of ξ_1 , while maintaining ξ_2 fixed at 0.04. At a length of 5.2, the frequency shift is 1.47, which increases to $8.11 \cdot 10^3$ at a length of 40.2 for $\xi_1 = 0.4$. Similarly, the frequency shift increases from $3.21 \cdot 10^{-1}$ to $1.66 \cdot 10^2$ as ξ_1 varies from 0 to 0.8 for a length of 10.2. It is evident that the value of frequency shift increases with the increase in length and the non-local parameter ξ_1 .

Table 2. Frequency shift for different lengths keeping fixed $\xi_2 = 0.04$

$\xi_1 \backslash L$	0.2	5.2	10.2	15.2	20.2	25.2	30.2	35.2	40.2	45.2
0	$1.78 \cdot 10^{-8}$	1.13	$3.21 \cdot 10^{-1}$	5.57	34.9	$1.20 \cdot 10^2$	$3.33 \cdot 10^2$	$6.89 \cdot 10^2$	$1.19 \cdot 10^3$	$1.61 \cdot 10^3$
0.4	$1.86 \cdot 10^{-8}$	1.47	60.2	$3.30 \cdot 10^2$	$9.02 \cdot 10^2$	$1.87 \cdot 10^3$	$3.33 \cdot 10^3$	$5.38 \cdot 10^3$	$8.11 \cdot 10^3$	$1.16 \cdot 10^4$
0.6	$4.19 \cdot 10^{-8}$	3.29	$1.13 \cdot 10^2$	$5.35 \cdot 10^2$	$1.41 \cdot 10^3$	$2.89 \cdot 10^3$	$5.07 \cdot 10^3$	$8.08 \cdot 10^3$	$1.21 \cdot 10^4$	$1.73 \cdot 10^4$
0.8	$7.45 \cdot 10^{-8}$	5.80	$1.66 \cdot 10^2$	$7.32 \cdot 10^2$	$1.89 \cdot 10^3$	$3.77 \cdot 10^3$	$6.47 \cdot 10^3$	$1.02 \cdot 10^4$	$1.50 \cdot 10^4$	$2.12 \cdot 10^4$

Table 3. Damping for different lengths keeping fixed $\xi_1 = 0.5$

$\xi_2 \backslash L$	0.2	5.2	10.2	15.2	20.2	25.2	30.2	35.2	40.2	45.2
0	$9.09 \cdot 10^{-19}$	$9.67 \cdot 10^{-4}$	$3.64 \cdot 10^2$	0.153	0.367	0.327	0.321	0.0329	0.348	0.383
0.4	$7.30 \cdot 10^{-18}$	$8.14 \cdot 10^{-3}$	$6.45 \cdot 10^2$	0.281	0.666	0.398	0.358	0.353	0.366	0.399
0.6	$1.62 \cdot 10^{-17}$	$1.32 \cdot 10^{-2}$	$7.39 \cdot 10^2$	0.324	0.763	0.413	0.365	0.358	0.370	0.402
0.8	$2.81 \cdot 10^{-17}$	$1.54 \cdot 10^{-2}$	$7.78 \cdot 10^2$	0.341	0.8	0.419	0.368	0.359	0.371	0.403

Table 3 illustrates the variation of damping for different lengths with different values of ξ_2 , while keeping ξ_1 fixed at 0.5. At a length of 10.2, the damping value is $7.39 \cdot 10^{-2}$, which increases to $4.02 \cdot 10^{-1}$ at a length of 45.2 for $\xi_2 = 0.6$. Similarly, damping increases from $3.21 \cdot 10^{-1}$ to $3.68 \cdot 10^{-1}$ as ξ_2 varies from 0 to 0.8 for a length of 30.2. This analysis highlights the trend where the damping value increases with the increase in length.

Table 4 displays the variation of frequency shift for different lengths with different values of ξ_2 , while maintaining ξ_1 fixed at 0.5. At a length of 10.2, the frequency shift is $1.70 \cdot 10^2$, which increases to $1.33 \cdot 10^5$ at a length of 45.2 for $\xi_2 = 0.0$. Similarly, the frequency shift increases from $7.49 \cdot 10^2$ to $5.32 \cdot 10^3$ as ξ_2 varies from 0 to 0.8 for a length of 15.2. It is evident that the value of frequency shift increases with the increase in length and the non-local parameter ξ_2 .

Table 5 presents damping values for different thicknesses while fixing ξ_2 at 0.04. Four values of ξ_1 are considered: 0, 0.2, 0.6 and 0.8, with thickness ranging from 0.2 to 1. The table reveals a trend where damping decreases as thickness increases and increases with ξ_1 .

Table 4. Frequency shift for different lengths keeping fixed $\xi_1 = 0.5$

$\xi_2 \backslash L$	0.2	5.2	10.2	15.2	20.2	25.2	30.2	35.2	40.2	45.2
0	$1.88 \cdot 10^{-7}$	5.86	$1.70 \cdot 10^2$	$7.49 \cdot 10^2$	$1.77 \cdot 10^3$	$6.98 \cdot 10^3$	$1.89 \cdot 10^4$	$4.11 \cdot 10^4$	$7.77 \cdot 10^4$	$1.33 \cdot 10^5$
0.4	$4.18 \cdot 10^{-7}$	3.03	$3.86 \cdot 10^2$	$1.62 \cdot 10^3$	$3.87 \cdot 10^3$	$2.27 \cdot 10^4$	$6.73 \cdot 10^4$	$1.52 \cdot 10^5$	$2.93 \cdot 10^5$	$5.07 \cdot 10^5$
0.6	$4.25 \cdot 10^{-7}$	5.51	$7.56 \cdot 10^2$	$3.15 \cdot 10^3$	$7.59 \cdot 10^3$	$4.92 \cdot 10^4$	$1.48 \cdot 10^5$	$3.37 \cdot 10^5$	$6.53 \cdot 10^5$	$1.13 \cdot 10^6$
0.8	$4.13 \cdot 10^{-7}$	7.97	$1.27 \cdot 10^3$	$5.32 \cdot 10^3$	$1.29 \cdot 10^4$	$8.63 \cdot 10^4$	$2.61 \cdot 10^5$	$5.97 \cdot 10^5$	$1.16 \cdot 10^6$	$2.00 \cdot 10^6$

Table 5. Damping for different thickness keeping fixed $\xi_2 = 0.04$

$\xi_1 \backslash h$	0.2	0.25	0.3	0.35	0.4	0.45	0.5	0.55	0.6
0	1.12	0.714	0.32	0.273	0.111	$2.76 \cdot 10^{-2}$	$1.31 \cdot 10^{-2}$	$7.35 \cdot 10^{-3}$	$4.51 \cdot 10^{-3}$
0.2	0.768	0.267	0.33	$2.91 \cdot 10^{-3}$	$4.78 \cdot 10^{-3}$	$5.46 \cdot 10^{-3}$	$4.45 \cdot 10^{-3}$	$3.38 \cdot 10^{-3}$	$2.58 \cdot 10^{-3}$
0.6	1.81	1.13	0.719	0.477	0.333	0.255	0.212	0.176	0.138
0.8	2.93	1.93	1.28	0.876	0.631	0.495	0.422	0.366	0.302
$\xi_1 \backslash h$	0.65	0.7	0.75	0.8	0.85	0.9	0.95	1	
0	$3.01 \cdot 10^{-3}$	$4.02 \cdot 10^{-2}$	$1.88 \cdot 10^{-3}$	$1.22 \cdot 10^{-3}$	$8.8 \cdot 10^{-4}$	$6.32 \cdot 10^{-4}$	$7.63 \cdot 10^{-4}$	$4.78 \cdot 10^{-4}$	
0.2	$2.0 \cdot 10^{-3}$	$1.55 \cdot 10^{-3}$	$1.22 \cdot 10^{-3}$	$9.79 \cdot 10^{-4}$	$8.0 \cdot 10^{-4}$	$6.66 \cdot 10^{-4}$	$5.63 \cdot 10^{-4}$	$4.84 \cdot 10^{-4}$	
0.6	0.103	$7.48 \cdot 10^{-2}$	$5.4 \cdot 10^{-2}$	$3.95 \cdot 10^{-2}$	$2.91 \cdot 10^{-2}$	$2.17 \cdot 10^{-2}$	$1.64 \cdot 10^{-2}$	$1.26 \cdot 10^{-2}$	
0.8	0.236	0.177	0.132	$9.76 \cdot 10^{-2}$	$7.29 \cdot 10^{-2}$	$5.51 \cdot 10^{-2}$	$4.21 \cdot 10^{-2}$	$3.25 \cdot 10^{-2}$	

For instance, damping decreases from 2.93 to 1.12 as ξ_1 decreases from 0.8 to 0 for a thickness of 0.2. Conversely, damping decreases from $3.38 \cdot 10^{-3}$ to $1.12 \cdot 10^{-3}$ with the increase in thickness from 0.5 to 0.75 at $\xi_1 = 0.2$. This observation underscores the inverse relationship between damping and thickness, and the direct relationship between damping and the non-local parameter ξ_1 .

Table 6 presents various frequency shift values for different thicknesses and ξ_1 , with a fixed value of $\xi_2 = 0.04$. At a thickness of 0.25, the frequency shift is $1.75 \cdot 10^4$, which decreases to $1.73 \cdot 10^5$ at a thickness of 0.95 for $\xi_1 = 0.0$. Similarly, the frequency shift increases from $2.0 \cdot 10^4$ to $5.42 \cdot 10^4$ as ξ_1 varies from 0 to 0.8 for a thickness of 0.35. It is evident that the frequency shift decreases with an increase in thickness and increases with an increased value of the non-local parameter ξ_1 .

Table 6. Frequency Shift for different Thickness keeping fixed $\xi_2 = 0.04$

$\xi_1 \backslash h$	0.2	0.25	0.3	0.35	0.4	0.45	0.5	0.55	0.6
0	2.29 $\cdot 10^5$	3.1 $\cdot 10^4$	1.83 $\cdot 10^4$	2.0 $\cdot 10^4$	6.93 $\cdot 10^3$	6.31 $\cdot 10^3$	5.16 $\cdot 10^3$	4.19 $\cdot 10^3$	3.43 $\cdot 10^3$
0.2	4.45 $\cdot 10^4$	1.75 $\cdot 10^4$	5.17 $\cdot 10^3$	2.49 $\cdot 10^3$	3.81 $\cdot 10^3$	4.4 $\cdot 10^3$	4.23 $\cdot 10^3$	3.88 $\cdot 10^3$	3.5 $\cdot 10^3$
0.6	1.97 $\cdot 10^5$	1.06 $\cdot 10^5$	6.66 $\cdot 10^4$	4.65 $\cdot 10^4$	3.49 $\cdot 10^4$	2.73 $\cdot 10^4$	2.21 $\cdot 10^4$	1.81 $\cdot 10^4$	1.52 $\cdot 10^4$
0.8	2.26 $\cdot 10^5$	1.23 $\cdot 10^5$	7.76 $\cdot 10^4$	5.42 $\cdot 10^4$	4.08 $\cdot 10^4$	3.24 $\cdot 10^4$	2.65 $\cdot 10^4$	2.22 $\cdot 10^4$	1.89 $\cdot 10^4$
$\xi_1 \backslash h$	0.65	0.7	0.75	0.8	0.85	0.9	0.95	1	
0	2.84 $\cdot 10^3$	2.89 $\cdot 10^3$	1.98 $\cdot 10^3$	1.68 $\cdot 10^3$	1.44 $\cdot 10^3$	1.25 $\cdot 10^3$	1.08 $\cdot 10^3$	9.43 $\cdot 10^2$	
0.2	3.14 $\cdot 10^3$	2.83 $\cdot 10^3$	2.55 $\cdot 10^3$	2.3 $\cdot 10^3$	2.08 $\cdot 10^3$	1.9 $\cdot 10^3$	1.73 $\cdot 10^3$	1.58 $\cdot 10^3$	
0.6	1.3 $\cdot 10^4$	1.12 $\cdot 10^4$	9.76 $\cdot 10^3$	8.61 $\cdot 10^3$	7.66 $\cdot 10^3$	6.86 $\cdot 10^3$	6.18 $\cdot 10^3$	5.6 $\cdot 10^3$	
0.8	1.63 $\cdot 10^4$	1.42 $\cdot 10^4$	1.25 $\cdot 10^4$	1.1 $\cdot 10^4$	9.83 $\cdot 10^3$	8.83 $\cdot 10^3$	7.98 $\cdot 10^3$	7.24 $\cdot 10^3$	

Table 7. Damping for different thickness keeping fixed $\xi_1 = 0.5$

$\xi_2 \backslash h$	0.2	0.25	0.3	0.35	0.4	0.45	0.5	0.55	0.6
0	1.18	0.323	0.155	0.102	6.47 $\cdot 10^{-2}$	3.98 $\cdot 10^{-2}$	2.58 $\cdot 10^{-2}$	1.76 $\cdot 10^{-2}$	1.22 $\cdot 10^{-2}$
0.2	2.3	1.57	1.15	0.92	0.806	0.754	0.727	0.705	0.677
0.6	2.37	1.63	1.2	0.977	0.877	0.848	0.854	0.876	0.902
0.8	2.37	1.63	1.21	0.981	0.881	0.853	0.862	0.887	0.918
$\xi_2 \backslash h$	0.65	0.7	0.75	0.8	0.85	0.9	0.95	1	
0	8.61 $\cdot 10^{-3}$	6.23 $\cdot 10^{-3}$	4.59 $\cdot 10^{-3}$	3.44 $\cdot 10^{-3}$	2.61 $\cdot 10^{-3}$	2.01 $\cdot 10^{-3}$	1.57 $\cdot 10^{-3}$	1.24 $\cdot 10^{-3}$	
0.2	0.642	0.599	0.549	0.496	0.442	0.389	0.339	0.294	
0.6	0.928	0.951	0.969	0.983	0.991	0.994	0.99	0.981	
0.8	0.949	0.981	1.01	1.03	1.05	1.07	1.08	1.09	

Table 7 presents various values of damping for different thicknesses and ξ_2 , with a fixed value of $\xi_1 = 0.5$. The damping value increases from $9.77 \cdot 10^{-1}$ to $9.94 \cdot 10^{-1}$ with an increase in thickness from 0.35 to 0.9 for $\xi_2 = 0.6$. Conversely, damping decreases from $3.23 \cdot 10^{-1}$ to 1.63 with an increase in ξ_2 from 0 to 0.8 for a thickness of 0.25.

The Table 8 lists various frequency shift values for different thicknesses and ξ_2 , with a fixed value of $\xi_1 = 0.5$. At a thickness of 0.3, the frequency shift is 9878118.5, which decreases to 71532.1 at a thickness of 0.85 for $\xi_2 = 0.8$. Similarly, the frequency shift increases from 36698.3 to 432373 as ξ_2 varies from 0 to 0.8 for a thickness of 0.6. It is evident that the frequency shift decreases with an increase in thickness and increases with an increased value of the non-local parameter ξ_2 .

Table 8. Frequency shift for different thickness keeping fixed $\xi_1 = 0.5$

$\frac{h}{\xi_2}$	0.2	0.25	0.3	0.35	0.4	0.45	0.5	0.55	0.6
0	2883508	1290230	644145	348412	200973	122490	78422.1	52529.4	36698.3
0.2	$1.1 \cdot 10^7$	5049251	2490816	1324891	747222	442257	272814	174542	115398
0.6	$2.6 \cdot 10^7$	$1.1 \cdot 10^7$	5568845	2952666	1658042	975718	597432	378641	247411
0.8	$4.5 \cdot 10^7$	$2 \cdot 10^7$	9878118	5231594	2933246	1722637	1051994	664500	432373
$\frac{h}{\xi_2}$	0.65	0.7	0.75	0.8	0.85	0.9	0.95	1	
0	26665.5	20093.3	15650.9	12556	10335.5	8696.03	7451.61	6481.94	
0.2	78627.7	55094.4	39635.2	29236.6	22088.3	17074.3	13490.3	10881.9	
0.6	166154	114399	80591.2	57997.4	42582.1	31864	24281.4	18830.4	
0.8	288861	197622	138150	98504.1	71532.1	52839.8	39664.4	30232.6	

Table 9. Damping and frequency shifts for different lengths keeping fixed $\xi_2 = 0.04$

$\xi_2 = 0.04$												
	L	0.2	5.2	10.2	15.2	20.2	25.2	30.2	35.2	40.2	45.2	
ξ_1	0	$4.32 \cdot 10^{-22}$	$6.52 \cdot 10^{-6}$	$1.32 \cdot 10^{-7}$	$1.40 \cdot 10^{-5}$	$1.82 \cdot 10^{-4}$	$1.85 \cdot 10^{-3}$	$2.93 \cdot 10^{-3}$	$4.56 \cdot 10^{-3}$	$8.87 \cdot 10^{-3}$	$3.45 \cdot 10^{-2}$	Damping
		$1.78 \cdot 10^{-8}$	1.13	0.321	5.57	34.9	120	333	689	$1.19 \cdot 10^3$	$1.61 \cdot 10^3$	Frequency shift
	0.4	$7.66 \cdot 10^{-21}$	$2.32 \cdot 10^{-5}$	$8.52 \cdot 10^{-4}$	$3.11 \cdot 10^{-3}$	$8.61 \cdot 10^{-3}$	$1.90 \cdot 10^{-2}$	$3.53 \cdot 10^{-2}$	$5.99 \cdot 10^{-2}$	$9.15 \cdot 10^{-2}$	0.128	Damping
		$1.86 \cdot 10^{-8}$	1.47	60.2	330	902	$1.87 \cdot 10^3$	$3.33 \cdot 10^3$	$5.38 \cdot 10^3$	$8.11 \cdot 10^3$	$1.16 \cdot 10^4$	Frequency shift
	0.6	$5.82 \cdot 10^{-20}$	$8.26 \cdot 10^{-5}$	$1.78 \cdot 10^{-3}$	$5.95 \cdot 10^{-3}$	$1.45 \cdot 10^{-2}$	$3.08 \cdot 10^{-2}$	$5.76 \cdot 10^{-2}$	$9.33 \cdot 10^{-2}$	0.137	0.191	Damping
		$4.19 \cdot 10^{-8}$	3.29	113	535	$1.41 \cdot 10^3$	$2.89 \cdot 10^3$	$5.07 \cdot 10^3$	$8.08 \cdot 10^3$	$1.21 \cdot 10^4$	$1.73 \cdot 10^4$	Frequency shift
	0.8	$2.45 \cdot 10^{-19}$	$1.83 \cdot 10^{-4}$	$2.59 \cdot 10^{-3}$	$8.24 \cdot 10^{-3}$	$1.95 \cdot 10^{-2}$	$4.44 \cdot 10^{-2}$	$8.27 \cdot 10^{-2}$	0.136	0.208	0.304	Damping
		$7.45 \cdot 10^{-8}$	5.8	166	732	$1.89 \cdot 10^3$	$3.77 \cdot 10^3$	$6.47 \cdot 10^3$	$1.02 \cdot 10^4$	$1.5 \cdot 10^4$	$2.12 \cdot 10^4$	Frequency shift

Table 10. Damping and frequency shifts for different thickness keeping fixed $\xi_1 = 0.5$

$\xi_1 = 0.5$												
	h	0.2	0.25	0.3	0.35	0.4	0.45	0.5	0.55	0.6	0.65	
ξ_2	0	1.18	0.323	0.155	0.102	$6.47 \cdot 10^{-2}$	$3.98 \cdot 10^{-2}$	$2.58 \cdot 10^{-2}$	$1.76 \cdot 10^{-2}$	$1.22 \cdot 10^{-2}$	$8.61 \cdot 10^{-2}$	Damping
		$2.88 \cdot 10^6$	$1.29 \cdot 10^6$	$6.44 \cdot 10^6$	$3.48 \cdot 10^5$	$2 \cdot 10^5$	$1.22 \cdot 10^5$	$7.8 \cdot 10^4$	$5.25 \cdot 10^4$	$3.67 \cdot 10^4$	$2.67 \cdot 10^4$	Frequency shift
	0.2	2.30	1.57	1.15	0.92	0.806	0.754	0.727	0.705	0.677	0.642	Damping
		$1.1 \cdot 10^7$	$5.05 \cdot 10^6$	$2.5 \cdot 10^6$	$1.3 \cdot 10^6$	$7.47 \cdot 10^5$	$4.4 \cdot 10^5$	$2.73 \cdot 10^5$	$1.74 \cdot 10^5$	$1.15 \cdot 10^5$	$7.86 \cdot 10^4$	Frequency shift
	0.6	2.37	1.63	1.20	0.977	0.877	0.848	0.854	0.876	0.902	0.928	Damping
		$2.6 \cdot 10^7$	$1.1 \cdot 10^7$	$5.57 \cdot 10^6$	$2.95 \cdot 10^6$	$1.66 \cdot 10^6$	$9.76 \cdot 10^5$	$5.97 \cdot 10^5$	$3.8 \cdot 10^5$	$2.47 \cdot 10^5$	$1.66 \cdot 10^5$	Frequency shift
	0.8	2.37	1.63	1.21	0.981	0.881	0.853	0.862	0.887	0.918	0.949	Damping
		$4.5 \cdot 10^7$	$2 \cdot 10^7$	$9.87 \cdot 10^6$	$5.2 \cdot 10^6$	$2.9 \cdot 10^6$	$1.72 \cdot 10^6$	$10.5 \cdot 10^5$	$6.64 \cdot 10^5$	$4.32 \cdot 10^5$	$2.9 \cdot 10^5$	Frequency shift

Case (I): Figs. 1–4 demonstrate the variations of damping and frequency shift with respect to length for non-local parameters. Here we take $h = 0.2$, $\alpha^* = 0.025$. In Figs. 1, 2, $\xi_2 = 0.04$ and in Figs. 3, 4, $\xi_1 = 0.5$.

Figure 1 shows the variation of damping with different Lengths. In this figure, the non-local parameter ξ_1 varies for four different values i.e. 0.0, 0.4, 0.6 and 0.8. It can be observed that the value of damping increases from 0.00085 to 0.035338 for $\xi_1 = 0.4$ as length increases from 10.2 to 30.2. Also, it can be observed that the value of damping increases from 0.00595 to 0.00824 for 15.2 length as ξ_1 increases from 0.6 to 0.8.

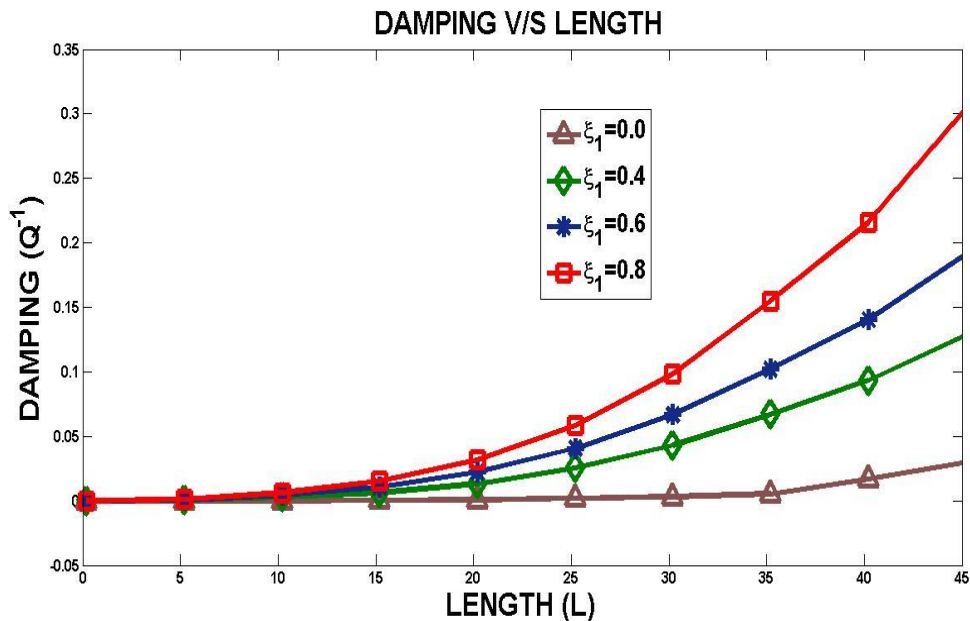
**Fig. 1.** Damping V/S length for $\xi_2 = 0.04$

Figure 2 depicts the graph showing the relationship between frequency shift and length, with the length varying from 0 to 45.2. The graph indicates that the damping value increases from 1.47081457 at a length of 5.2 to 1865.83847 when the length extends to 25.2 for $\xi_1 = 0.4$. This analysis reveals that an increase in length results in a higher damping quality factor.

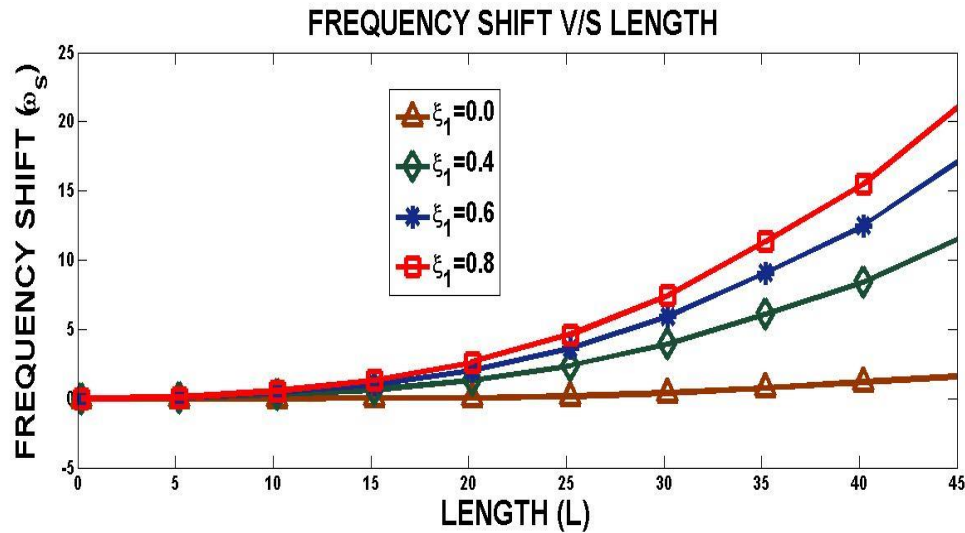


Fig. 2. Frequency shift V/S lengths for $\xi_2 = 0.04$

Figure 3 depicts the graph illustrating the relationship between damping and length, with the value of ξ_1 fixed at 0.5. In this graph, ξ_2 is set at four different values: 0, 0.4, 0.6, and 0.8. It is evident that the damping value increases with an increase in length, and damping also increases with the increase in the value of ξ_2 .

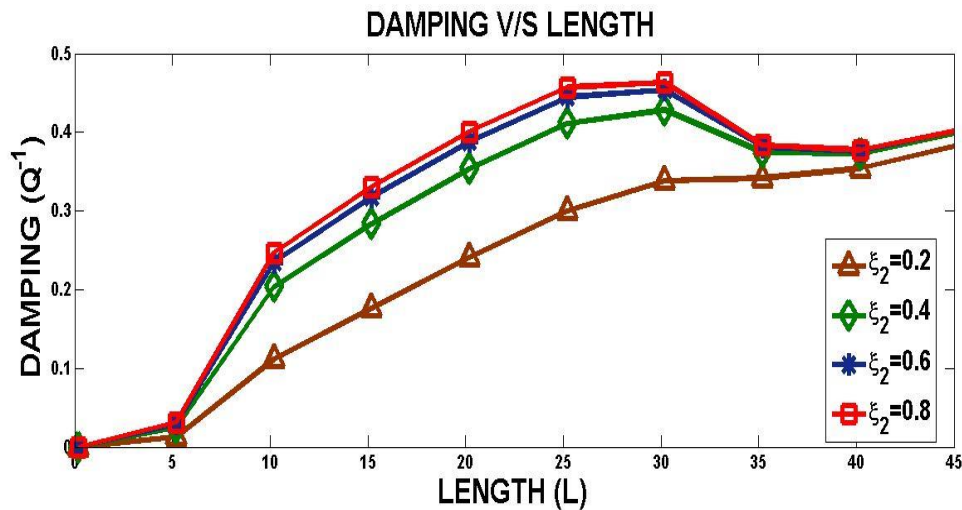


Fig. 3. Damping V/S length for $\xi_1 = 0.5$

Figure 4 presents the relationship between frequency shift and length, with the length varying from 0 to 45. The graph clearly shows that the frequency shift value increases from 1274.7908 at a length of 10.2 to 2004762.9366 when the length extends to 45.2 for $\xi_1 = 0.8$. This analysis indicates that an increase in length results in a higher frequency shift.

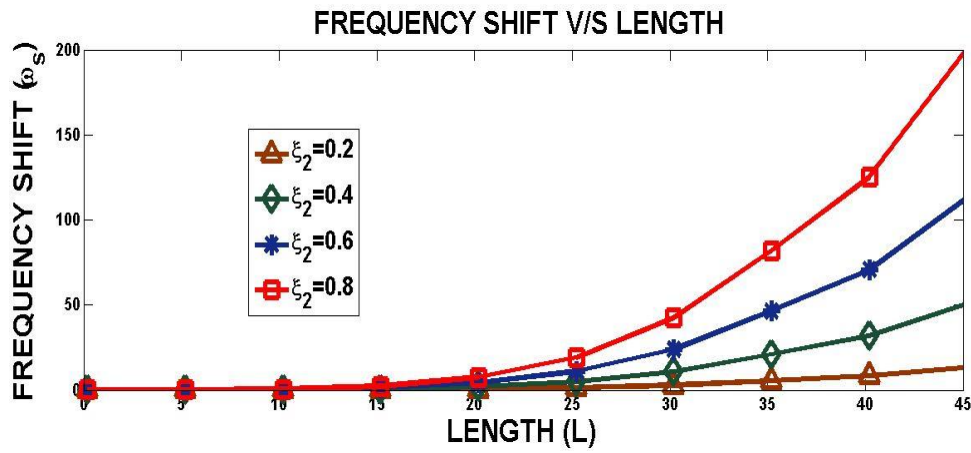


Fig. 4. Frequency shift V/S lengths for $\xi_1 = 0.5$

Case (II): Figures 5–8 demonstrate the variations of damping and frequency shift with respect to thickness for non-local parameters. Here we take $L = 100$, $\alpha^* = 0.025$. In Figs. 5, 6, $\xi_2 = 0.04$, and in Figs. 7, 8, $\xi_1 = 0.5$.

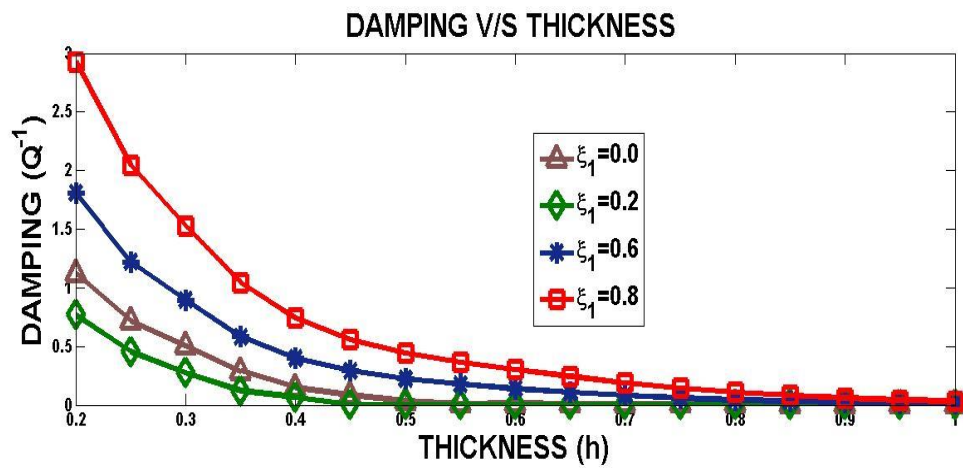


Fig. 5. Damping V/S thickness for $\xi_2 = 0.04$

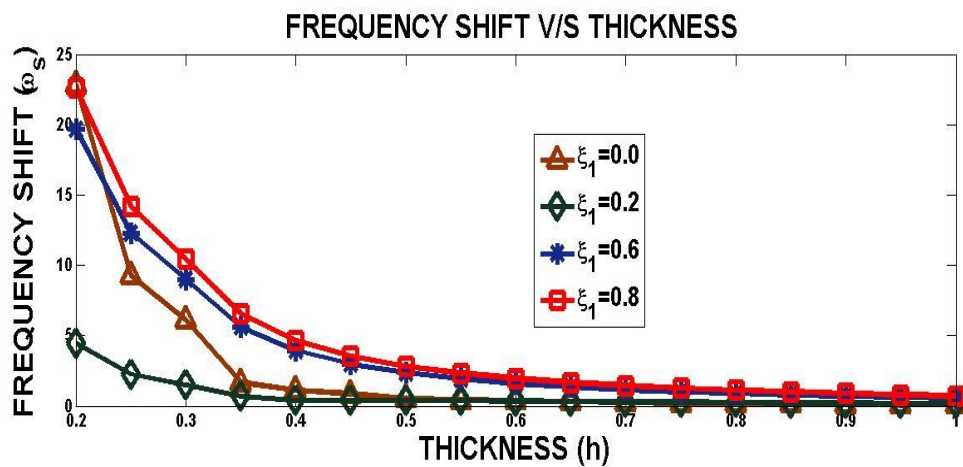


Fig. 6. Frequency shift V/S thickness for $\xi_2 = 0.04$

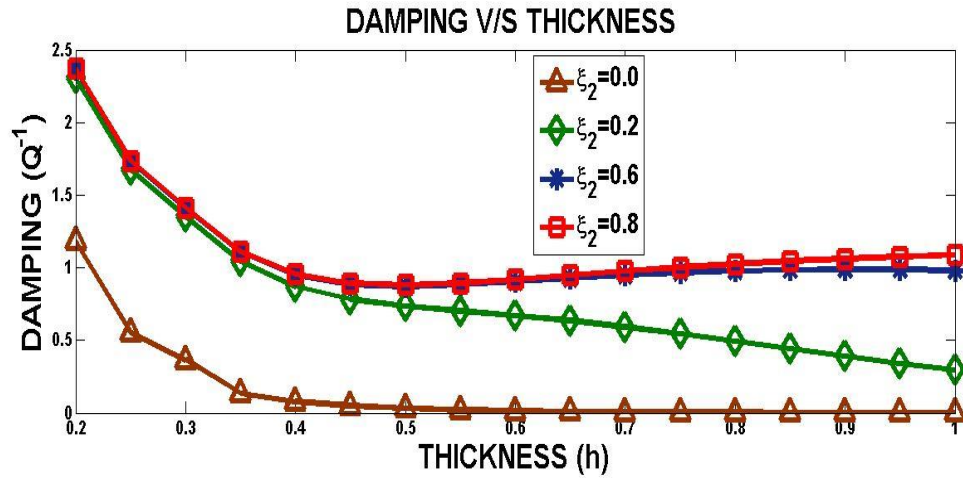


Fig. 7. Damping V/S thickness for $\xi_1 = 0.5$

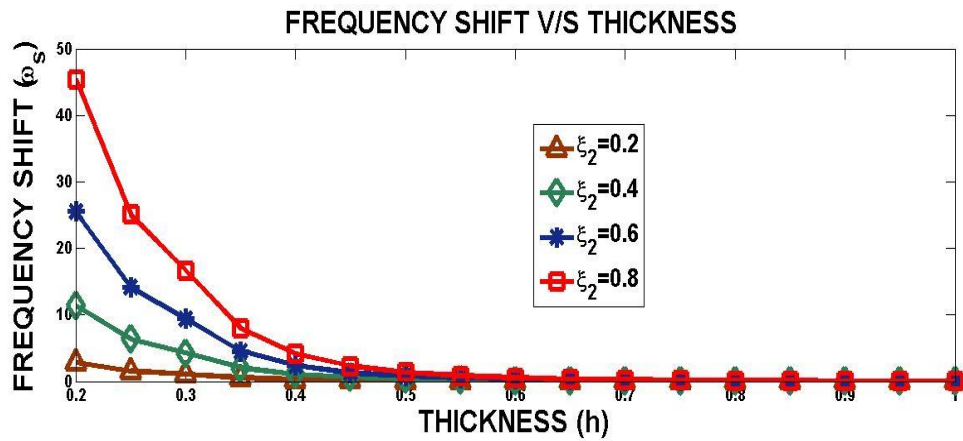


Fig. 8. Frequency shift V/S thickness for $\xi_1 = 0.5$

Figure 6 shows the graph of frequency shift versus thickness. In this graph, the thickness varies from 0.0 to 1. It can be easily observed that the value of frequency shift is 5168.949742 at a thickness of 0.3 and decreases to 2545.67 at a thickness of 0.75 for $\xi_1 = 0.2$. The frequency shift increases from 4194.238 to 22205.95 as ξ_1 varies from 0 to 0.8 for a thickness of 0.55. By analysing this graph, it is found that an increase in thickness results in a decrease in the damping quality factor, but the frequency shift increases as the non-local parameter ξ_1 increases.

Figure 7 illustrates the relationship between damping and thickness, with the value of ξ_1 fixed at 0.5. In this graph, ξ_2 is set at four different values: 0, 0.2, 0.6 and 0.8. It can be observed that the damping value increases with an increase in thickness, while the damping decreases as the non-local parameter ξ_2 increases.

Figure 8 shows the graph of frequency shift versus thickness. By analysing this graph, it is found that an increase in thickness results in a decrease in the frequency shift, but the frequency shift increases with the increased value of the non-local parameter ξ_2 .

Case (III): Figures 9–12 explain the variations of damping and frequency shift with respect to length and thickness for non-local parameters with varying empirical material constant $\alpha^* = 0, 0.001, 0.004, 0.008$, $\xi_1 = 0.5$, $\xi_2 = 0.04$.

In Figs. 9 and 10, $h = 0.2$, and in Figs. 11 and 12, $L = 100$. Figures 9 and 10 illustrate

the TDP effect. It can be easily analysed from these graphs that the damping quality factor and frequency shift increases with increasing length. It is also observed that with the increase in empirical material constant (α^*), the damping and frequency shift decreases.

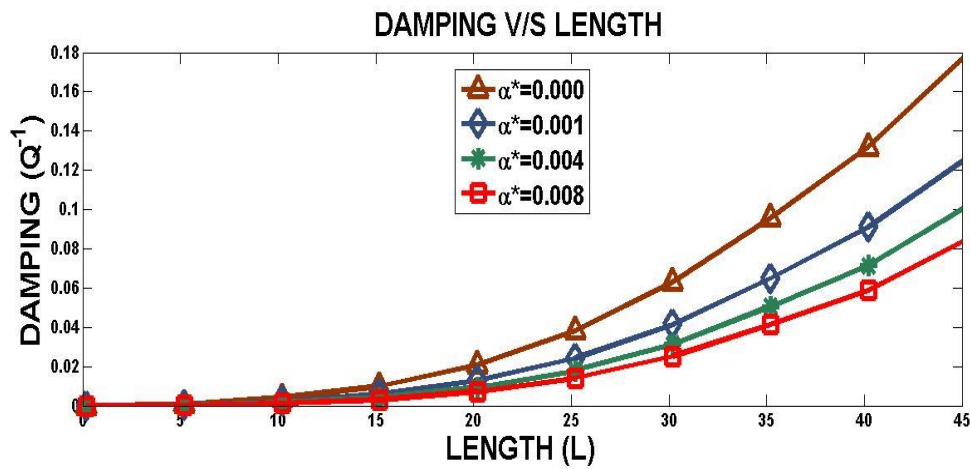


Fig. 9. Damping V/S length with TDP effect

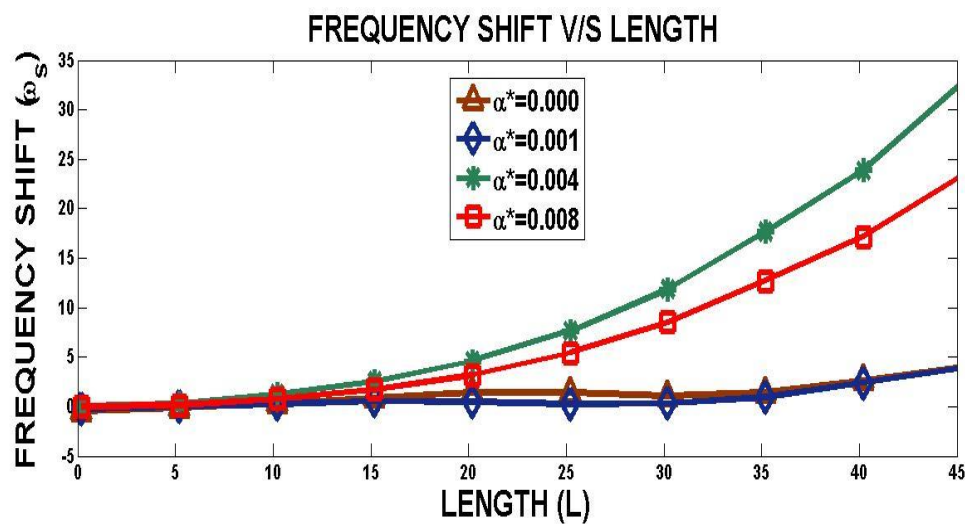


Fig. 10. Frequency shift V/S length with TDP effect

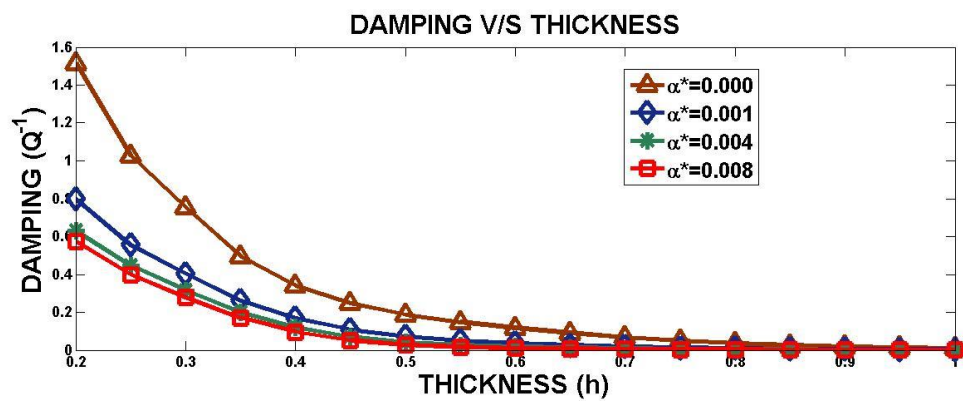


Fig. 11. Damping V/S thickness with TDP effect

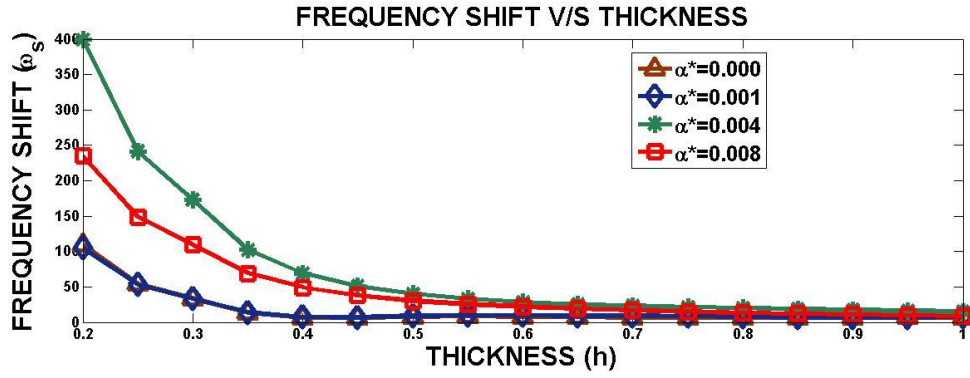


Fig. 12. Frequency shift V/S thickness with TDP effect

Figures 11 and 12 show the TDP effect. It can be analysed from these graphs that the damping and frequency shift value reduces with increasing thickness. It is also observed that with the increase in empirical material constant (α^*), the damping and frequency shift decreases.

Case (IV): Figures 13–16 demonstrate the LS and DPL models in the variations of damping and frequency shift for $\xi_1 = 0.05$, $\xi_2 = 0.04$, $\tau_t = 0$, $\tau_q = 0.05$, $\alpha^* = 0.025$. In Figs. 13 and 14, $h = 0.2$, and in Figs. 15 and 16, $L = 100$.

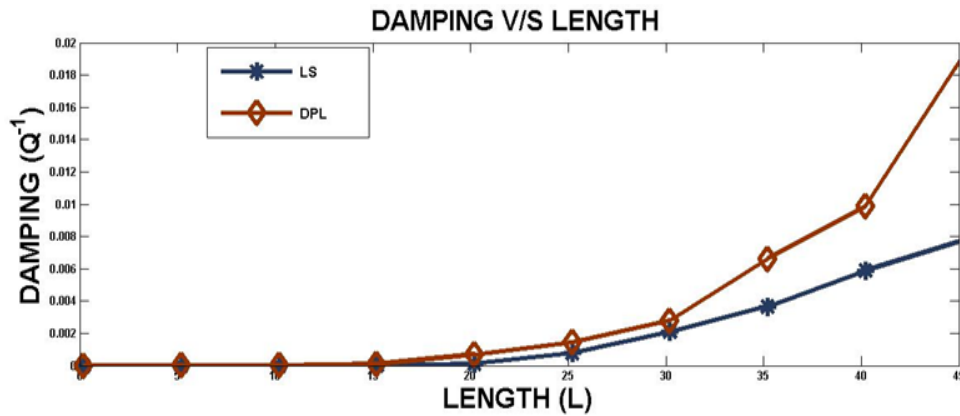


Fig. 113. Comparison of LS and DPL for damping V/S length

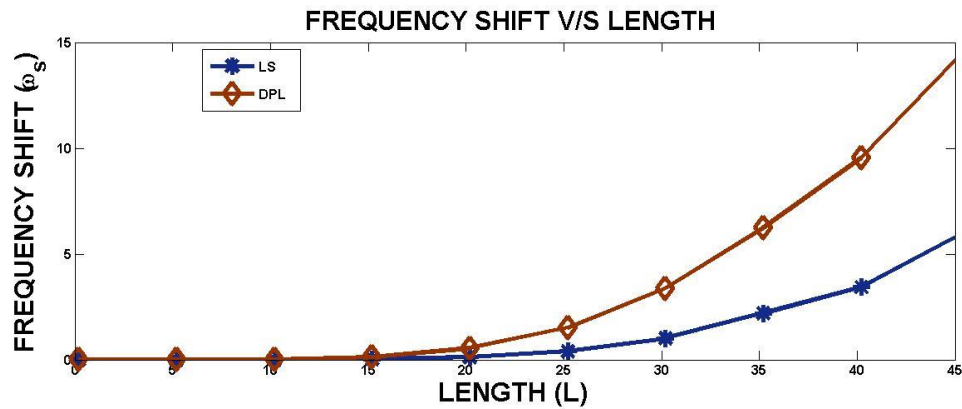


Fig. 124. Comparison of LS and DPL for frequency shift V/S length

The comparison of damping and frequency shift versus length are shown in Figs. 13 and 14. It can be seen that the damping factor and frequency shift for LS is less than for DPL. For both the LS and DPL models, the damping quality factor and frequency shift rises with increase in length.

In Figs. 15 and 16, the comparison of damping and frequency shift versus thickness are shown. In the instance of DPL theory, the damping factor and frequency shift has been observed to be higher than in LS models. The damping factor and frequency shift decreases with increase in thickness for both the LS and DPL models.

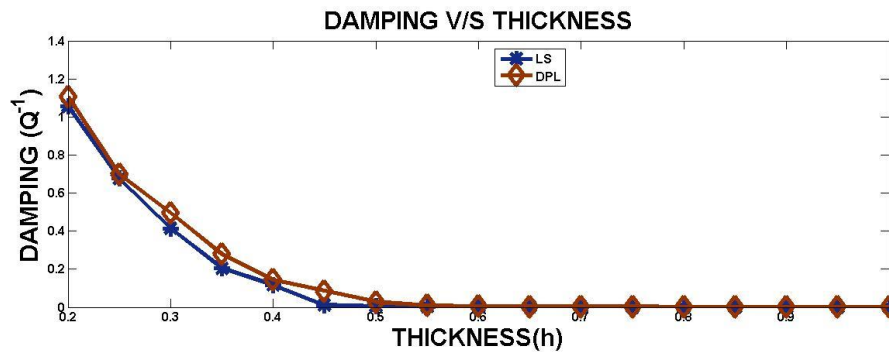


Fig. 135. Comparison of LS and DPL for damping V/S thickness

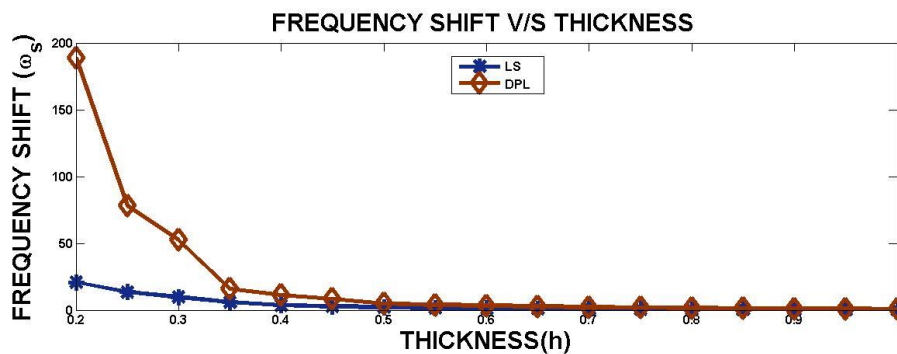


Fig. 146. Comparison of LS and DPL for frequency shift V/S thickness

Conclusions





Traditional models assume classical (local) elasticity, where stress at a point depends only on strain at that same point. The suggested model includes non-local elasticity, which accounts for size-dependent effects-essential for modelling materials at small scales, where classical theories become inaccurate. The advancement is to capture scale effects relevant to micro/nano-structures, improving the precision of stress and strain predictions. The present study investigates thermoelastic damping (TD) and frequency shift (FS) in Kirchhoff plates, considering thermoelastic theory under the influence of non-local parameters, dual-phase lag, and temperature-dependent properties. TD and FS are analysed under simply supported boundary conditions. The results are tabulated and displayed graphically with varying values of length and thickness to explore the impacts of non-local parameters, temperature dependent parameters and the comparison between LS and DPL models. It is observed that the damping quality factor and FS

increase with the increase in non-local parameters ξ_1 and ξ_2 and decreases with increasing thickness with distinct magnitude.

Damping and frequency shift are likewise detected under the TDP effect, and they increase with length. Additionally, it is noted that the damping and frequency shift diminish as the empirical material constant (α^*) increases. These graphs show also it is observed that as thickness increases, magnitude of damping and frequency shift decrease under the impact of TDP. The damping quality factor and frequency shift increase with length for both the DPL and LS versions although magnitude of these field variables for LS remains smaller than DPL.

It is concluded that the impact of non-local and temperature dependent parameters play a valuable role in processing and characterisation to improve the material property. The work presented here is useful for the researcher working in thermodynamics, engineering, material science and hyperbolic thermodynamic model.

CRediT authorship contribution statement

Rajneesh M. Kumar  : writing – review & editing, supervision, conceptualization;
Pooja Singhal  : writing – original draft, investigation, data curation

Conflict of interest

The authors declare that they have no conflict of interest.

References

1. Zener C. Internal Friction in Solids. *Physical Review*. 1937;52(3): 230–235.
2. Zener C. Internal friction in solids II. General theory of thermoelastic internal friction. *Physical Review*. 1938;53(1): 90–99.
3. Sun Y, Fang D, Soh AK. Thermoelastic damping in micro-beam resonators. *International Journal of Solids and Structures*. 2006;43(10): 3213–3229.
4. Eringen AC, Edelen DGB. On nonlocal elasticity. *International Journal of Engineering Science*. 1972;10(3): 233–248.
5. Eringen AC. Theory of nonlocal thermoelasticity. *International Journal of Engineering Science*. 1974;12(12): 1063–1077.
6. Yu YJ, Tian XG, Xiong QL. Nonlocal thermoelasticity based on nonlocal heat conduction and nonlocal elasticity. *European Journal of Mechanics - A/Solids*. 2016;60: 238–253.
7. Xu Y, Zhou D, Liu K. Three-dimensional thermoelastic analysis of rectangular plates with variable thickness subjected to thermomechanical loads. *Journal of Thermal Stresses*. 2010;33(12): 1136–1155.
8. Sun Y, Saka M. Thermoelastic damping in micro-scale circular plate resonators. *Journal of Sound and Vibration*. 2010;329(3): 328–337.
9. Grover D, Sharma JN. Transverse vibrations in piezothermoelastic beam resonators. *Journal of Intelligent Material Systems and Structures*. 2012;23(1): 77–84.
10. Alashti RA, Abolghasemi AH. A Size-dependent Bernoulli-Euler Beam Formulation based on a New Model of Couple Stress Theory. *International Journal of Engineering*. 2014;27(6): 951–960.
11. Sharma S, Sharma K. Influence of Heat Sources and Relaxation Time on Temperature Distribution in Tissues. *International Journal of Applied Mechanics and Engineering*. 2014;19(2): 427–433.
12. Abbas IA. Exact Solution of Thermoelastic Damping and Frequency Shifts in a Nano-Beam Resonator. *International Journal of Structural Stability and Dynamics*. 2015;15(6): 1–12.
13. Kumar R, Devi S, Sharma V. Damping in microscale modified couple stress thermoelastic circular Kirchhoff plate resonators. *Applications and Applied Mathematics*. 2017;12(2): 924–945.
14. Zhang H, Kim S, Choi G, Xie D, Cho HH. Effect of temperature dependent material properties on thermoelastic damping in thin beams. *International Journal of Heat and Mass Transfer*. 2019;139: 1031–1036.

15. Marin M, Öchsner A, Bhatti MM. Some results in Moore-Gibson-Thompson thermoelasticity of dipolar bodies. *ZAMM Zeitschrift für Angewandte Mathematik und Mechanik*. 2020;100(12): 1–13.
16. Borjalilou V, Asghari M, Taati E. Thermoelastic damping in nonlocal nanobeams considering dual-phase-lagging effect. *Journal of Vibration and Control*. 2020;26(11–12): 1042–1053.
17. Abouelregal AE, Marin M. The response of nanobeams with temperature-dependent properties using state-space method via modified couple stress theory. *Symmetry*. 2020;12(8): 1276.
18. Devi S. Thermoelastic Damping and Frequency Shift in Kirchhoff Plate Resonators Based on Modified Couple Stress Theory With Dual-Phase-Lag Model. *Journal of Stress Analysis*. 2020;12(3): 700–712.
19. Guha S, Singh AK. Frequency shifts and thermoelastic damping in different types of Nano-/Micro-scale beams with sandiness and voids under three thermoelasticity theories. *Journal of Sound and Vibration*. 2021;510: 116301.
20. Sharma S, Khator S. Power generation planning with reserve dispatch and weather uncertainties including penetration of renewable sources. *Smart Grid and Clean Energy*. 2021;10(4): 292–303.
21. Sharma S, Khator S. Micro-Grid Planning with Aggregator's Role in the Renewable Inclusive Prosumer Market. *Journal of Power and Energy Engineering*. 2022;10(4): 47–62.
22. Guha S, Singh AK. Frequency shifts and thermoelastic damping in distinct Micro-/Nano-scale piezothermoelastic fiber-reinforced composite beams under three heat conduction models. To be published in *Journal of Ocean Engineering and Science*. [Preprint] 2022. Available from: doi.org/10.1016/j.joes.2022.06.015.
23. Kaur I, Singh K. Functionally graded nonlocal thermoelastic nanobeam with memory-dependent derivatives. *SN Applied Sciences*. 2022;4(12): 312.
24. Kumar R, Devi S. The effects of two temperature and laser pulse on modified couple stress thermoelastic diffusion beam. *Engineering Solid Mechanics*. 2023;11(2): 217–230.
25. Huang D, Xiong H, Yang G. Analytical modeling and numerical analysis of thermoelastic damping in ultrathin elastic films due to surface effects. *Scientific Reports*. 2023;13(1): 46826.
26. Abouelregal AE, Marin M, Askar SS. Analysis of the magneto-thermoelastic vibrations of rotating Euler–Bernoulli nanobeams using the nonlocal elasticity model. *Boundary Value Problems*. 2023;2023(1): 1–23.
27. Ren X, Shi S. A Buckling Analysis of Thermoelastic Micro/Nano-Beams Considering the Size-Dependent Effect and Non-Uniform Temperature Distribution. *Materials*. 2023;16(19): 6390.
28. Selvamani R, Loganathan R, Yaylaci M, Yaylaci EU, Özdemir ME. Vibration of piezo-magneto-thermoelastic FG nanobeam submerged in fluid with variable nonlocal parameter. *Advanced Nano Research*. 2024;16(5): 489–500.
29. Sharma S, Sharma K, Bhargava RR. Wave motion and representation of fundamental solution in electro-microstretch viscoelastic solids. *Materials Physics and Mechanics*. 2013;17(2): 93–110.
30. Kumar R, Partap G. Propagation of waves in micropolar thermoelastic cubic crystals. *Applied Mathematics and Information Sciences*. 2010;4(1): 107–123.
31. Kumar R, Devi S, Sharma V. Plane waves and fundamental solution in a modified couple stress generalized thermoelastic with mass diffusion. *Materials Physics and Mechanics*. 2015;24(4): 72–85.
32. Lotfy K, Elidy ES, Tantawi RS. Photothermal Excitation Process during Hyperbolic Two-Temperature Theory for Magneto-Thermo-Elastic Semiconducting Medium. *Silicon*. 2021;13(7): 2275–2288.
33. Lotfy K, El-Bary AA, El-Sharif AH. Ramp-type heating microtemperature for a rotator semiconducting material during photo-excited processes with magnetic field. *Results in Physics*. 2020;19: 103338.
34. Lotfy K, El-Bary AA, Hassan W, Ahmed MH. Hall current influence of microtemperature magneto-elastic semiconductor material. *Superlattices and Microstructures*. 2020;139: 106428.
35. Alharbi AR, Almatrafi MB, Lotfy K. Constructions of solitary travelling wave solutions for Ito integro-differential equation arising in plasma physics. *Results in Physics*. 2020;19: 103533.
36. Lotfy K, El-Bary AA. Magneto-Photo-Thermo-Microstretch Semiconductor Elastic Medium Due to Photothermal Transport Process. *Silicon*. 2022;14(9): 4809–4821.
37. Ismail GM, Gepreel KA, Lotfy K, Mahdy AMS, El-Bary A, Saeed AM. Influence of variable thermal conductivity on thermal-plasma-elastic waves of excited microelongated semiconductor. *Alexandria Engineering Journal*. 2022;61(12): 12271–12282.
38. Abouelregal AE, Marin M, Foul A. Thermoviscoelastic Responses in Kirchhoff Circular Micro-Plate via MGT Thermoelastic Model and Modified Couple Stress Theory. *Mechanics of Solids*. 2024;59: 2269–2291.
39. Aldandani M, Abouelregal A. Study of Thermo-Viscoelastic Interactions in Microplates Resting on an Elastic Foundation and Subjected to External Loads Using DPL Thermoelastic Model. *Iranian Journal of Science and Technology, Transactions of Mechanical Engineering*. 2025;49: 217–233.

40. Abouelregal AE. Fibre-reinforced generalized anisotropic thick plate with initial stress under the influence of fractional thermoelasticity theory. *Advances in Applied Mathematics and Mechanics*. 2017;9(3): 722–741.
41. Abouelregal AE, Marin M, Foul A, Askar SS. Coupled responses of thermomechanical waves in functionally graded viscoelastic nanobeams via thermoelastic heat conduction model including Atangana – Baleanu fractional derivative. *Scientific Reports*. 2024;14(1): 58866.
42. Abouelregal AE, Elzayady ME, Marin M. Thermoelastic modeling of functionally graded materials with cylindrical cavities utilizing higher-order fractional heat transfer models incorporating time delays. *Continuum Mechanics and Thermodynamics*. 2025;37: 31.
43. Tzou DY, Guo ZY. Nonlocal behavior in thermal lagging. *International Journal of Thermal Sciences*. 2010;49(7): 1133–1137.
44. Rao SS. *Vibration of Continuous Systems*. Hoboken: Wiley; 2007.
45. Chen W, Li X. A new modified couple stress theory for anisotropic elasticity and microscale laminated Kirchhoff plate model. *Archive of Applied Mechanics*. 2014;84(3): 323–341.
46. Guo FL, Song J, Wang GQ, Zhou YF. Analysis of thermoelastic dissipation in circular micro-plate resonators using the generalized thermoelasticity theory of dual-phase-lagging model. *Journal of Sound and Vibration*. 2014;333(11): 2465–2474.
47. Sharma JN. Thermoelastic damping and frequency shift in micro/nanoscale anisotropic beams. *Journal of Thermal Stresses*. 2011;34(7): 650–666.